ORIGINAL ARTICLE

Effect of nitride addition on the electrical and thermal properties of pressureless solid-state sintered SiC ceramics

Rohit Malik[1] · Young-Wook Kim[1]

Abstract

SiC-0–8wt% Si_3N_4 and SiC-0–10 wt% TiN ceramics were fabricated via pressureless solid-state sintering using B_4C and C as sintering aids. Si_3N_4 and TiN addition up to 4 and 1 wt%, respectively exhibited ˃ 97% relative density. Thermal decomposition of nitrides and subsequent N_2 evolution during sintering resulted in the low relative densities at the high levels of nitride content. This study demonstrated that 0.5–1 wt% nitride addition led to three orders of magnitude increase ($10^5 \rightarrow 10^8$ cm^{-3}) in carrier density due to nitride-derived N-doping in SiC lattice and, consequently an order of magnitude decrease ($10^7 \rightarrow 10^6$ Ω•cm) in the electrical resistivity. An increased thermal resistance at SiC-nitride heterogeneous grain boundaries was responsible for ~ 32% decrease in thermal conductivity with 1 wt% nitride addition.

Keywords SiC · Pressureless solid-state sintering · Electrical properties · Thermal properties

1 Introduction

Silicon carbide (SiC) is an important structural material with unique engineering properties such as high temperature strength (> 600 MPa at 1600 °C), high flexural strength (200–950 MPa), high hardness (20–30 GPa), high fracture toughness (2–7.5 MPa·m$^{1/2}$) and tunable electrical (10^{-3}–10^{13} Ω·cm) and thermal (32–270 Wm^{-1} K^{-1}) properties [1–10]. Recently, there is growing interest in pressureless solid-state sintered (PSS) SiC ceramics due to their potential application in the fabrication of semiconductor processing parts such as, wafer boats, susceptors, focus rings, and dummy wafers [11–18].

PSS SiC ceramics are sintered using B and C as sintering aids in Ar gas or vacuum at $T > 2000$ °C [1, 2]. The role of B is to segregate at the grain boundaries and reduce the grain boundary energy (γ_{GB}) and C increases the surface energy (γ_{SV}) of SiC particles by removing the native SiO_2 film via a carbothermal reduction process. The combined effect of both additives reduces γ_{GB}/γ_{SV} to a subcritical value, thus making the densification process thermodynamically feasible.

Depending upon the processing conditions, additive content, purity and polytype of the starting powders, PSS SiC ceramics exhibit thermal conductivity of 50–190 Wm^{-1} K^{-1}, electrical resistivity of 10^6–10^{11} Ω·cm, hardness of 21–30 GPa, flexural strength of 200–556 MPa, and fracture toughness of 2.3–5.7 MPa·m$^{1/2}$ [11–18].

The high electrical resistivity (> 10^6 Ω cm) of PSS SiC ceramics restricts their electrodischarge machinability to fabricate intricate shaped parts used in the semiconductor processing industries [11, 17, 18]. The PSS SiC ceramics with a low electrical resistivity of 10^2 Ω cm were fabricated by adding electrically conductive graphene [17]. However, the carbon/graphene added PSS SiC ceramics are not suitable for fabricating semiconductor processing parts because of the deleterious effects of C on the subsequent CVD processing of the parts [19–24]. One potential solution to fabricate electrodischarge machinable PSS SiC ceramics is N-doping of SiC lattice. For instance, the electrical resistivity of liquid phase sintered (LPS) SiC ceramics could be reduced by ten orders of magnitude ($10^8 \rightarrow 10^{-2}$ Ω cm) by liquid phase assisted N-doping of SiC lattice [24]. The SiC lattice can be doped with N by (1) sintering in N_2 gas or (2) use of metallic/non-metallic nitrides as N-doping source [4, 19–24]. Given that N_2 gas hinders the mass transport leading to poor sintered densities in the PSS SiC ceramics [25], the use of secondary nitride phases could be a potential method to fabricate electrodischarge machinable PSS SiC ceramics.

✉ Young-Wook Kim
  ywkim@uos.ac.kr

1   Functional Ceramics Laboratory, Department of Materials
     Science and Engineering, The University of Seoul,
     Seoul 02504, Republic of Korea

In our previous work [26], AlN was shown to reduce the electrical resistivity of PSS SiC ceramics by four orders of magnitude from 1.7×10^5 Ω cm to 8.3×10^1 Ω·cm with 1 wt% AlN addition. However, Al-based compounds cannot be used to fabricate semiconductor processing parts because Al impurities could end up in the finished semiconductor products and deteriorate their performance. Thus, it is necessary to explore new nitride phases to reduce the electrical resistivity of PSS SiC ceramics.

This study investigates Si_3N_4 and TiN as potential novel nitride phases to reduce the electrical resistivity of PSS SiC ceramics. In LPS SiC ceramics, Si_3N_4 and TiN have been used to fabricate electrodischarge machinable SiC ceramics [19, 21]. In fact, 10 vol% Si_3N_4 content was sufficient to achieve two orders of magnitude decrease in the electrical resistivity ($1.3 \times 10^0 \rightarrow 9.0 \times 10^{-2}$ Ω·cm), which was attributable to an increased charge carrier density ($10^{19} \rightarrow 10^{20}$ cm^{-3}) caused by the Si_3N_4 derived N-doping in the SiC lattice. Similarly, LPS SiC-25 vol% TiN composites exhibited three orders of magnitude decrease ($10^{-1} \rightarrow 10^{-4}$ Ω·cm) in electrical resistivity due to the combined beneficial effect of TiN-derived N-doping in the SiC lattice and electrically conductive TiN grain boundaries [19]. Thus far, there are no investigations on the effect of Si_3N_4 and TiN phases on the electrical and thermal properties of PSS SiC ceramics. Given that the N-doping occurs via relatively slow solid-state diffusion process in PSS SiC ceramics compared to liquid phase diffusion during LPS process [25–27], it would be interesting to evaluate the effectiveness of nitrides derived N-doping in PSS SiC ceramics.

2 Experimental procedure

Commercially available α-SiC (0.5 μm, Sintex 15C, Sika Tech, Fiven, Norway), B_4C (0.5 μm, Kojundo Chemical Co., Ltd., Japan), phenolic resin (TD-739, Kangnam Chemical Co., Ltd., Korea), Si_3N_4 (~ 200 nm, Grade E10,

Ube Industries, Tokyo, Japan), and TiN (~ 1 μm, Grade C, H.C. Starck, Germany) were used as the starting materials. The phenolic resin had a carbon yield of 60%. As shown in Table 1, eight batches of powders with varying initial Si_3N_4 and TiN content were prepared. The baseline specimen was designated as ST0. The specimens with Si_3N_4 and TiN phases were designated as *S/Tx*, where '*S*', '*T*', and '*x*' denote Si_3N_4, TiN, and wt% of the nitride phase, respectively. B_4C and C contents were fixed at 0.7 and 2.5 wt%, respectively, in all batches based on our previous works [18, 19]. The batches were mixed by ball milling using SiC balls in ethanol with a ball to powder weight ratio of 2:1. After drying, the powder mixture was granulated using a 60-mesh sieve. The sieved powders were uniaxially pressed at 25 MPa into cylindrical (Ø 25 mm × 7 mm high) compacts, followed by cold isostatic pressing at 207 MPa. The green compacts were pyrolyzed at 900 °C in flowing Ar gas for 1 h and subsequently pressureless sintered in a graphite resistance furnace at 2100 °C for 2 h in flowing Ar gas. The theoretical density was determined using the rule of mixtures. The sintered density was determined using the weight-to-volume ratio of the sintered specimens. The polished specimens (up to 1 μm) were etched using a modified Murakami's reagent [28]. The characterization details of microstructure using SEM, phase analysis using XRD, electrical properties using Hall effect, thermal conductivity using laser flash method are described elsewhere [11, 13–15]. The grain size was defined as the average of longest and shortest diagonal passing through the grain centroid. The average grain size was analyzed using 300 grains for each specimen. The quantitative phase analysis of SiC polytypes was performed by Rietveld refinement method using a commercially available software (TOPAS, Bruker Corporation, USA).

Table 1 Batch composition**,** theoretical density, relative density, and weight loss during sintering in pressureless solid-state sintered SiC-Si_3N_4 and SiC-TiN ceramics

Specimen	Batch composition (wt%)	Theoretical density (g/cm^3)	Relative density (%)	Weight loss during sintering (%)
ST0	96.8% α−SiC+2.5% C+0.7% B_4C	3.173	98.2	1.5
S0.5	96.3% α−SiC+0.5% α−Si_3N_4+2.5% C+0.7% B_4C	3.173	97.9	1.6
S1	95.8% α−SiC+1% α−Si_3N_4+2.5% C+0.7% B_4C	3.173	97.8	1.7
S4	92.8% α−SiC+4% α−Si_3N_4+2.5% C+0.7% B_4C	3.173	97.5	3.0
S8	88.8% α−SiC+8% α−Si_3N_4+2.5% C+0.7% B_4C	3.172	62.8	5.1
T1	95.8% α−SiC+1% TiN+2.5% C+0.7% B_4C	3.186	97.3	2.9
T5	91.8% α−SiC+5% TiN+2.5% C+0.7% B_4C	3.238	58.1	3.2
T10	86.8% α−SiC+10% TiN+2.5% C+0.7% B_4C	3.305	55.6	4.0
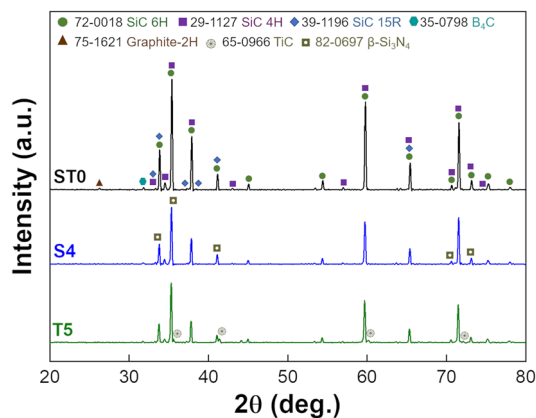
Fig. 1 XRD patterns of pressureless solid-state sintered SiC-Si$_3$N$_4$ and SiC-TiN ceramics (refer to Table 1)

Table 2 SiC polytype content in pressureless solid-state sintered SiC-Si$_3$N$_4$ and SiC-TiN ceramics

Specimen	SiC polytype content (wt%)		
	6H	4H	15R
ST0	86.0	10.1	3.9
S4	86.7	8.5	4.8
T5	89.4	4.5	6.1

3 Results and discussion

3.1 Phase analysis and microstructure

As shown in Table 1, the relative density decreased with increasing Si$_3$N$_4$ and TiN content. The partial decomposition of nitrides was responsible for increased weight loss and decreased relative density with increasing nitride content. Si$_3$N$_4$ decomposes at $T > 1600$ °C via the following reaction [29]:

$$Si_3N_4(s) \rightarrow 3Si\ (l) + 2N_2(g) \tag{1}$$
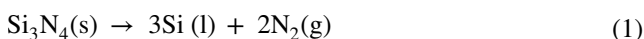
The Si$_3$N$_4$ content up to 4 wt% and TiN content up to 1 wt% resulted in > 97% relative density, whereas a further increase in nitride content resulted in large residual pores and very low relative density. Especially, the relative density drastically decreased to ~ 60% for nitride content ≥ 5 wt% presumably due to the deleterious effect of increased N$_2$ gas evolution during decomposition of nitrides. In a previous work [25], it was demonstrated that N$_2$ gas hinders the densification in PSS SiC ceramics. Fig. S1 shows the residual pores formed by the decomposition of nitride phases during sintering.

The XRD patterns and SiC polytype contents in the sintered specimens are shown in Fig. 1 and Table 2, respectively. The XRD patterns revealed α-SiC (6H, 4H, 15R

polytypes) and traces of TiC, Si$_3$N$_4$, graphite, and B$_4$C in the sintered specimens. TiC phase was detected in the TiN added specimen (T5, Fig. 1) presumably due to the reaction of the decomposing TiN with carbon during sintering via the following reaction:

$$2TiN\ (s) + 2C\ (s) \rightarrow 2TiC\ (s) + N_2(g) \tag{2}$$
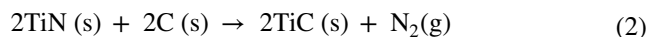
The Gibbs free energy of reaction (2) calculated using the JANAF tables [30] is − 62.258 kJ/mol. The graphite was formed at the sintering temperature by the graphitization of the residual C left after the carbothermal reduction of native SiO$_2$ [31]. The 4H-SiC content slightly decreased with the addition of nitrides presumably due to a low stability of 4H-SiC phase in the N-doped SiC lattice in SiC-nitride ceramics (Table 2). The literature reveals that p-type (Al, B) dopants and high temperature of sintering accelerate the 6H to 4H-SiC phase transformation [18, 26, 32]. However, there are no reports on the effect of N-doping (n-type dopants) on polytypic phase transformation in PSS SiC ceramics.

Typical microstructures of PSS SiC-nitrides ceramics are shown in Fig. 2. The SEM micrographs exhibited a coarse-grained microstructure with elongated α-SiC platelet grains formed via the preferential growth of α-SiC platelets along the basal plane. Si$_3$N$_4$ addition up to 4 wt% and TiN addition up to 1 wt% did not exhibit any change in the average grain size of SiC. The average grain size of SiC for ST0, S4 and T1 were 3.7 ± 1.8, 3.7 ± 1.9, and 3.8 ± 2.1, respectively.
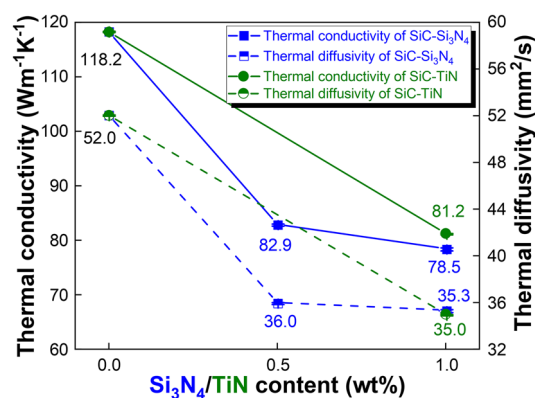
3.2 Electrical and thermal properties

The electrical resistivity and carrier density of PSS SiC-nitride ceramics are shown in Fig. 3. The electrical resistivity decreased by an order of magnitude from 6.8×10^7 Ω cm to 3.5×10^6 Ω·cm on adding 0.5 wt% Si$_3$N$_4$ because of the Si$_3$N$_4$ derived N-doping in the SiC lattice, which resulted in an increased carrier density from 2.2×10^5 cm^{-3} in ST0 to 2.0×10^8 cm^{-3} in S0.5. With a further increase in Si$_3$N$_4$ content, the electrical resistivity was increased to 8.5×10^6 Ω·cm at 1 wt% Si$_3$N$_4$ content due to the deleterious effect of electrically insulating Si$_3$N$_4$ grains [21]. Furthermore, the hall-effect measurement revealed a p-type conduction in the B-doped ST0. On the contrary, the nitride-derived N-doping resulted in an n-type conduction in the nitride added specimens. It was attributable to the three times higher solubility of N in SiC lattice than that of B [33]. S4 exhibited an electrical resistivity of > 10^8 Ω·cm, which could not be measured accurately due to the limitation (10^{-4}–10^7 Ω·cm) of the hall-effect measurement. Similarly, 1 wt% TiN addition was also beneficial in reducing ($6.8 \times 10^7 \rightarrow 9.0 \times 10^6$ Ω·cm) the electrical resistivity by an order of magnitude.

Fig. 2 Typical microstructures of pressureless solid-state sintered SiC-Si$_3$N$_4$ and SiC-TiN ceramics: **a** ST0, **b** S1, **c** S4, and **d** T1
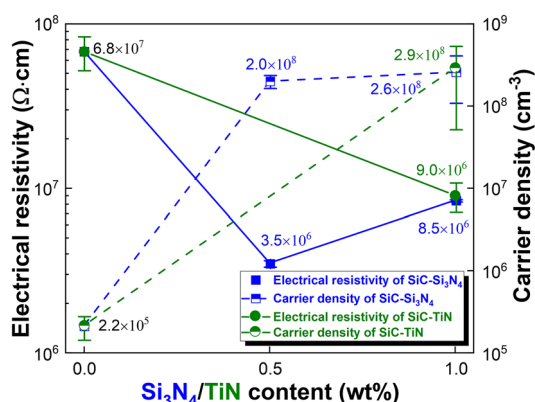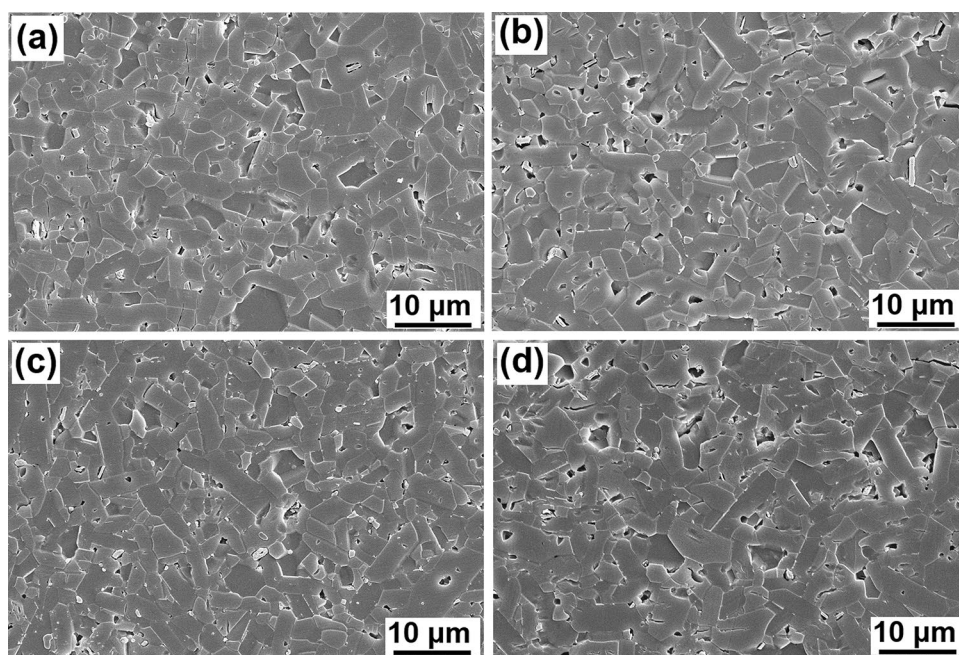
Fig. 3 Electrical resistivity and carrier density of pressureless solid-state sintered SiC-Si$_3$N$_4$ and SiC-TiN ceramics

Fig. 4 Thermal conductivity and thermal diffusivity of pressureless solid-state sintered SiC-Si$_3$N$_4$ and SiC-TiN ceramics

These findings are consistent with LPS SiC-1 wt% Si$_3$N$_4$ ceramics that also exhibited an order of magnitude reduction in electrical resistivity [21]. Thus, there is no significant effect of the relatively slow N-diffusivity during solid-state sintering compared to that in LPS process. Notably, for LPS SiC-0–25 vol% TiN composites [19], the electrical resistivity could be decreased by three orders of magnitude due to the combined beneficial effects of nitride phase derived N-doping in the SiC lattice and electrically conductive TiN grains. On the contrary, this study revealed that the low refractory nitride phases, such as TiN decomposes at the high processing temperature and thus, are not suitable for reducing the electrical resistivity of PSS SiC ceramics via nitride phase derived N-doping.

Given the low solubility (~ 0.5 wt%, 2200 °C) of N in SiC lattice [33], this study has demonstrated that a small amount (≤ 1 wt%) of nitride phase is sufficient to reduce the electrical resistivity of PSS SiC ceramics by an order of magnitude via N-doping. Whereas, the high nitride content leads to increased evolution of nitrogen gas and thus, hinders the densification process, as explained previously [25]. Furthermore, it is anticipated that the electrically conductive transition metal borides/carbides with excellent refractoriness could be potential candidates to fabricate electrically conductive PSS SiC composites, which will be investigated in future works.

The thermal conductivity and thermal diffusivity of PSS SiC-nitride ceramics are shown in Fig. 4. The

thermal conductivity monotonically decreased from 118.2 $Wm^{-1} K^{-1}$ in ST0 to 78.5 $Wm^{-1} K^{-1}$ in S4 predominantly due to an increased interfacial thermal resistance with increasing heterogeneous SiC-Si_3N_4 grain boundaries, which is also indicated by a gradual decrease in thermal diffusivity form 52 mm^2/s in ST0 to 35.3 mm^2/s in S1. Similarly, 1 wt% TiN addition was equally detrimental to thermal conductivity. Although the intrinsic thermal conductivity of TiN (190 $Wm^{-1} K^{-1}$) is higher than that of Si_3N_4 (43 $Wm^{-1} K^{-1}$) [34, 35], both nitride phases exhibited a similar thermal conductivity (~ 80 $Wm^{-1} K^{-1}$) on 1 wt% addition implying that the interfacial thermal resistance at the heterogeneous interfaces is the predominant factor in controlling the thermal conductivity of PSS SiC ceramics. It is also supported that the carrier contribution to thermal conduction was negligible (0.01–2.03%) in SiC-Zr_2CN composites [22]. The thermal conductivity of newly developed ceramics is comparable to that (83.6 $Wm^{-1} K^{-1}$) of PSS SiC-0.9 wt% BN ceramics [27].

4 Conclusions

Pressureless solid-state sintered (PSS) SiC-0–8 wt% Si_3N_4 and SiC-0–10 wt% TiN ceramics were sintered at 2100 °C for 2 h in flowing Ar gas using 0.7 wt% B_4C and 2.5 wt% C. The major findings are summarized as follows:

1. PSS SiC-0–4 wt% Si_3N_4 and SiC-1 wt% TiN ceramics exhibited ˃97% relative density. Thermal decomposition of nitride phase and subsequent N_2 evolution during sintering resulted in large residual pores and poor relative density at the high levels of nitride content.
2. XRD analysis revealed a low stability of 4H-SiC in the N-doped PSS SiC ceramics. TiN was transformed to TiC during sintering by reacting with carbon.
3. The microstructure of PSS SiC ceramics consisted of elongated α-SiC platelet grains. The SiC grain size was constant at ~ 3.7 μm irrespective of the nitride content in SiC-0–4 wt% Si_3N_4 and SiC-1 wt% TiN ceramics.
4. The electrical resistivity decreased from 6.8×10^7 to 3.5×10^6 Ω·cm on adding 0.5 wt% Si_3N_4 due an increased charge carrier density ($2.2 \times 10^5 \rightarrow 2.0 \times 10^8$ Ω·cm) caused by the Si_3N_4 derived N-doping in SiC lattice. Thereafter, the electrical resistivity increased to 8.5×10^6 Ω·cm with 1 wt% Si_3N_4 addition due to the increased content of electrically insulating Si_3N_4 grain boundaries. Similarly, TiN-derived N-doping led to one order of magnitude reduction in the electrical resistivity. The SiC-1 wt% TiN ceramic had an electrical resistivity of 9.0×10^6 Ω·cm.
5. The thermal conductivity monotonically decreased from 118.2 to 78.5 $Wm^{-1} K^{-1}$ with an increase in Si_3N_4 con-

tent from 0 to 4 wt% due to the increased interfacial thermal resistance at SiC-nitride heterogeneous interfaces. Similarly, the thermal conductivity was reduced to 81.2 $Wm^{-1} K^{-1}$ on adding 1 wt% TiN.

Declarations

References

1. S. Prochazka, in *Sintering of silicon carbide*, ed. By A.R. Cooper, A.H. Heuer. (Springer, Boston, 1975), p. 421–431
2. S. Prochazka, R.M. Scanlan, Effect of boron and carbon on sintering of SiC. J. Am. Ceram. Soc. **58**, 72 (1975)
3. Y.W. Kim, R. Malik, in *SiC ceramics, structure, processing, and properties*. ed. by M. Pomeroy (Elsevier, Amsterdam, 2020), pp. 150–164
4. Y.W. Kim, Y.H. Kim, K.J. Kim, Electrical properties of liquid-phase sintered silicon carbide ceramics: a review. Crit. Rev. Solid State Mater. Sci. **45**, 66–84 (2020)
5. T. Maity, Y.W. Kim, High-temperature strength of liquid-phase-sintered silicon carbide ceramics: a review. Int. J. Appl. Ceram. Technol. **19**, 130–148 (2022)
6. H. Wu, Y. Yan, G. Liu, X. Liu, Y. Zhu, Z. Huang, D. Jiang, Y. Li, Effects of grain grading on microstructures and mechanical behaviors of pressureless solid-state-sintered SiC. Int. J. Appl. Ceram. Technol. **12**, 976–984 (2015)
7. K. Raju, D.H. Yoon, Sintering additives for SiC based on the reactivity: a review. Ceram. Int. **42**, 17947–17962 (2016)
8. A. Noviyanto, D.H. Yoon, Y.H. Han, T. Nishimura, Effect of sintering atmosphere on the grain growth and hardness of SiC/polysilazane ceramic composites. Adv. Appl. Ceram. **115**, 272–275 (2016)
9. R.H. Ryu, K.S. Lee, Y.W. Kim, Indentation and contact damages on grain boundary controlled silicon carbide ceramics. J. Mater. Sci. **44**, 1416–1420 (2009)
10. S.M. Lee, T.W. Kim, H.J. Lim, C. Kim, Y.W. Kim, K.S. Lee, Mechanical properties and contact damages of nanostructured silicon carbide ceramics. J. Ceram. Soc. Jpn. **115**, 304–309 (2007)
11. W.D.G. Boecker, L.N. Hailey, C.H. McMurtry, Sintered silicon carbide ceramic body of high electrical resistivity. United States patent **4701427**, 20 (1985)
12. G. Magnani, G. Beltrami, G.L. Minoccari, L. Pilotti, Presureless sintering and properties of α-SiC-B_4C composite. J. Eur. Ceram. Soc. **21**, 633–638 (2001)
13. Y. Chen, L. Jiang, X. Jia, Properties of pressureless sintered SiC-TiB_2 composites. Adv. Mater. Res. **177**, 369–372 (2011)

14. Y. Li, J. Yin, H. Wu, P. Lu, Y. Yan, X. Liu, Z. Huang, D. Jiang, High thermal conductivity in pressureless densified SiC ceramics with ultra-low contents of additives derived from novel boron-carbon sources. J. Eur. Ceram. Soc. **34**, 2591–2595 (2014)

15. G. Magnani, A. Brentari, E. Burresi, G. Raiteri, Pressureless sintered silicon carbide with enhanced mechanical properties obtained by the two-step sintering method. Ceram. Int. **40**, 1759–1763 (2014)

16. Q. Li, Y. Zhang, H. Gong, H. Sun, T. Li, X. Guo, S. Ai, Effects of graphene on the thermal conductivity of pressureless-sintered SiC ceramics. Ceram. Int. **41**, 13547–13552 (2015)

17. N. Cai, D. Guo, G. Wu, F. Xie, S. Tan, N. Jiang, H. Li, Decreasing resistivity of silicon carbide ceramics by incorporation of graphene. Materials **13**, 3586 (2020)

18. R. Malik, Y.W. Kim, Effect of initial α-phase content on properties of pressureless solid-state sintered SiC ceramics. Int. J. Appl. Ceram. Technol. (2021). https://doi.org/10.1111/ijac.13892

19. T.Y. Cho, R. Malik, Y.W. Kim, K.J. Kim, Electrical and mechanical properties of pressureless sintered SiC-Ti$_2$CN composites. J. Eur. Ceram. Soc. **38**, 3064–3072 (2018)

20. R. Malik, H.M. Kim, Y.W. Kim, K.J. Kim, Grain-growth-induced high electrical conductivity in SiC–BN composites. Ceram. Int. **44**, 16394–16399 (2018)

21. H.J. Yeom, Y.W. Kim, K.J. Kim, Electrical, thermal, and mechanical properties of silicon carbide-silicon nitride composites sintered with yttria and scandia. J. Eur. Ceram. Soc. **35**, 77–86 (2015)

22. S.H. Jang, Y.W. Kim, K.J. Kim, Electrical and thermal properties of SiC-Zr$_2$CN composites sintered with Y$_2$O$_3$-Sc$_2$O$_3$ additives. J. Eur. Ceram. Soc. **37**, 477–484 (2017)

23. K.J. Kim, Y.W. Kim, K.Y. Lim, T. Nishimura, E. Narimatsu, Electrical and thermal properties of SiC-AlN ceramics without sintering additives. J. Eur. Ceram. Soc. **35**, 2715–2721 (2015)

24. Y.W. Kim, T.Y. Cho, K.J. Kim, Effect of grain growth on electrical properties of silicon carbide ceramics sintered with gadolinia and yttria. J. Eur. Ceram. Soc. **5**, 4137–4142 (2015)

25. Y. Taki, M. Kitiwan, H. Katsui, T. Goto, Effect of B doping on electrical and thermal properties of SiC bodies fabricated by spark plasma sintering. Mater. Today: Proc. **16**, 211–215 (2019)

26. R. Malik, Y.W. Kim, Effect of AlN addition on the electrical resistivity of pressureless sintered SiC ceramics with B$_4$C and C. J. Am. Ceram. Soc. **104**, 6086–6091 (2021)

27. R. Malik, Y.W. Kim, Pressureless solid-state sintering of SiC ceramics with BN and C additives. J. Asian Ceram. Soc. **9**, 1165–1172 (2021)

28. Z.A. Yasar, R.A. Haber, Effect of carbon addition and mixture method on the microstructure and mechanical properties of silicon carbide. Materials **13**, 3768 (2020)

29. H.D. Batha, E.D. Whitney, Kinetics and mechanism of thermal decomposition of Si$_3$N$_4$. J. Am. Ceram. Soc. **56**, 365–369 (1973)

30. M.W. Chase, C.A. Davies, I.R. Downey, A.J. Frurip, R.A. McDonald, A.N. Syverud, JANAF thermochemical tables—third edition. J. Phys. Chem. Ref. Data. **14**, 1 (1985)

31. R. Hamminger, Carbon inclusions in sintered silicon carbide. J. Am. Ceram. Soc. **72**, 1741–1744 (1989)

32. H. Tanaka, N. Hirosaki, T. Nishimura, D.W. Shin, S.S. Park, Non-equiaxial grain growth and polytype transformation of sintered α-silicon carbide and β-silicon carbide. J. Am. Ceram. Soc. **86**, 2222–2224 (2003)

33. S.A. Reshanov, I.I. Parfenova, V.P. Rastegaev, Group III-V impurities in β-SiC: lattice distortions and solubility. Diamond Relat. Mater. **10**, 1278–1282 (2001)

34. Azo materials, Silicon nitride properties and applications. (2021). https://www.azom.com/properties.aspx?ArticleID=53. Accessed 30 Oct 2021

35. Enigmatics, CVD of titanium nitride and other barrier metals. (2021). http://www.enigmatic-consulting.com/semiconductor_processing/CVD_Fundamentals/films/TiN.html. Accessed 30 Oct 2021